

## Design of a Free-Space Optical Communication Module for Small Satellites

Ryan Kingsbury, Kathleen Riesing, Prof. Kerri Cahoy  
 Space Systems Laboratory, Massachusetts Institute of Technology  
 77 Massachusetts Avenue, Cambridge, MA 02139  
 kingryan@mit.edu

### ABSTRACT

Free-space optical (FSO) communication technology has the potential to provide power-efficient communication links for small satellites that outperform traditional radio frequency approaches. Extremely high-gain apertures at optical carrier frequencies enable significantly improved performance. We present a design for a miniaturized CubeSat-scale optical transmitter capable of supporting downlink rates up to at least 10 Mbps. Our design incorporates a fine-steering mechanism that augments the capabilities of the host spacecraft's attitude determination and control system. In this work, we develop an optical layout that optimizes link performance metrics while staying within the size, weight, and power constraints of a payload within a standard 3U CubeSat. The selection criteria for critical components (detectors, optical sources, and steering mechanisms) are described. Simulation results showing sufficient beacon tracking performance (better than  $\pm 210 \mu\text{rad}$  3- $\sigma$ ) are presented. Finally, single-axis simulation results are shown for the staged pointing control system that show the benefits of the fine stage.

### INTRODUCTION

Free-space optical (FSO) communications offer many advantages over traditional radio frequencies (RF). Higher-gain apertures enable reductions in size, weight, and power (SWaP), as well as substantially reduced regulatory burden. For systems with severe SWaP constraints, such as nanosatellites, FSO offers significant potential.

To achieve the benefits of FSO, however, the FSO module must be pointed with extremely high accuracy. The requirements that FSO places on the pointing, acquisition, and tracking (PAT) subsystem are the major limiting factors in designing FSO systems. While successful communications links have been demonstrated ranging from LEO to GEO to lunar orbit [10, 13], existing solutions generally do not scale well to small platforms. The PAT subsystem typically relies on a two-stage approach, in which a coarse stage (e.g. two-axis gimballed terminal) is augmented by a higher-bandwidth fine stage (e.g. a fast steering mirror). In the case of a small satellite, the communications payload cannot rely on the capabilities of the host spacecraft; rather, the architecture must be modified to meet stringent SWaP requirements.

A recent effort has been made by the Aerospace Corporation to develop a FSO downlink on a CubeSat platform, the Optical Communications and Sensor Demonstration (OCS) [5]. OCS, set to launch in 2015, relies

on the body pointing of the CubeSat for single-stage control. Predicted pointing accuracy is 0.1 degrees to 0.7 degrees, depending on the control mode. For a baseline downlink of 5 Mbps (50 Mbps stretch), the optical power output is 14 W. OCS is near the limits of what can be achieved with a single-stage control approach.

Therefore, we describe the development of a FSO module for small satellites that employs two-stage control. The coarse control is achieved through body pointing and performance is augmented with a fine stage FSM for attitude correction. The system is designed to achieve at least a 10 Mbps downlink at 1 W optical output. The subsequent sections first describe the requirements of the FSO module, followed by the system architecture to achieve these goals. The uplink and downlink designs are addressed, along with their predicted performance. Finally, future work towards realizing this design is discussed.

### FSO SYSTEM REQUIREMENTS

#### *Platform Constraints*

In recent years, the capabilities of the attitude determination and control subsystem (ADCS) for small satellites have improved tremendously, enabling a class of CubeSat missions that require 3-axis stabilization. Key improve-

ments include commercial off-the-shelf (COTS) attitude control solutions using reaction wheels and magnetorquers, as well as improved accuracy of attitude determination sensors such as fine sun sensors, CMOS imagers and star trackers [2].

Although 3-axis stabilized CubeSats are still in early development, several missions have already demonstrated pointing accuracy of 3 degrees or better [5, 14, 1]. Proposed missions predict even higher accuracy. These include the Aerospace Corporation’s OCS mission with accuracy to 0.1 degrees, and the MIT/JPL/Draper Laboratory’s ExoplanetSat, which employs two-stage control to achieve an accuracy of 0.001 degrees [12].

With the goal of developing an optical downlink for nominal CubeSat missions, and our approach of using a staged control system, we assume that the CubeSat bus is capable of pointing within  $\pm 2.5$  degrees ( $3\text{-}\sigma$ ). Given the current capabilities, this number is reasonable for a 3-axis stabilized CubeSat mission, and it provides a baseline for our fine stage control design.

### Link Requirements

In order for FSO communication technologies to be useful, they must be competitive with existing RF-based solutions. Commercial radio modems are available for CubeSats which provide downlink rates in excess of 2 Mbps while consuming approximately 10 W of electrical power [7, 6]. Existing RF technology drives our self-imposed requirement for a  $> 10$  Mbps downlink data rate. A simple radiometric analysis of the optical downlink channel was conducted to assess feasibility of this goal. This analysis, presented in detail in Appendix A, assumes a 1 W optical transmitter on-board the satellite, conservative estimates for optics and atmospheric losses, a 1000 km path length and a baseline receiver performance of 1000 photons per bit. The downlink beam divergence, which is the system parameter that trades FSO link throughput with fine pointing capability, was adjusted until the desired 10 Mbps link rate was achieved. The result of this analysis was a 2.1 mrad beamwidth (0.12 deg).

### Pointing, Acquisition and Tracking Requirements

Based on the 2.1 mrad beamwidth and the link requirements described, the transmitted beam must be pointed with sub-milliradian accuracy. This sets the requirement on the fine stage at 1/10th of the beamwidth, or  $\pm 210 \mu\text{rad}$  ( $3\text{-}\sigma$ ).

The acquisition and tracking requirements are derived from the satellite orbit. To design a module applicable to a wide range of CubeSat missions, we conducted a survey of nominal orbits for CubeSat missions aided by results from previous surveys [6]. As seen in Figure 1, due to the recent increase in International Space Station (ISS) launches, the ISS orbit has become the most common. For the purposes of designing the FSO system, lower altitude orbits place more stringent requirements on an FSO module due to higher slew rates during communication. Therefore, the FSO module is designed for a 400 km circular orbit, which drives steering and tracking capabilities that support a range of orbits from 400 km and higher.

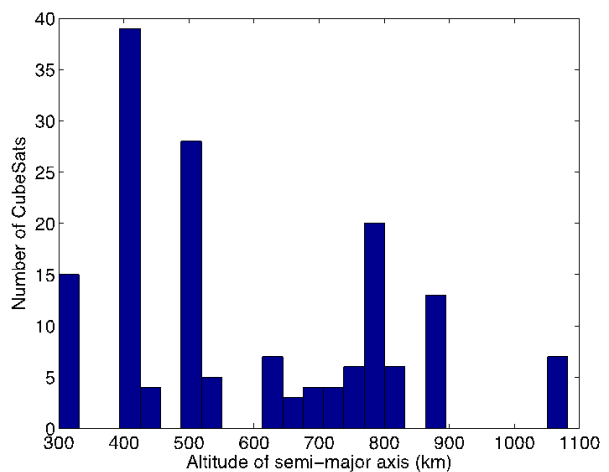


Figure 1: Histogram of all prior CubeSat orbits

For orbits from 400 km to 700 km, the downlink pass duration is on the order of several minutes. This drives our requirement that the link must be acquired within one minute. In terms of tracking, the CubeSat (as well as the ground station) must support slew rates of up to about 1 degree/s while maintaining the required pointing accuracy of the link.

## FSO SYSTEM ARCHITECTURE

### Optical Layout

A bistatic configuration, which consists of separate transmit and receive apertures, has been selected for the design (Figure 2). This design approach decouples the two optical paths and allows the design parameters of each path, particularly field of view and divergence, to be tailored to the specific requirements of the uplink and downlink.

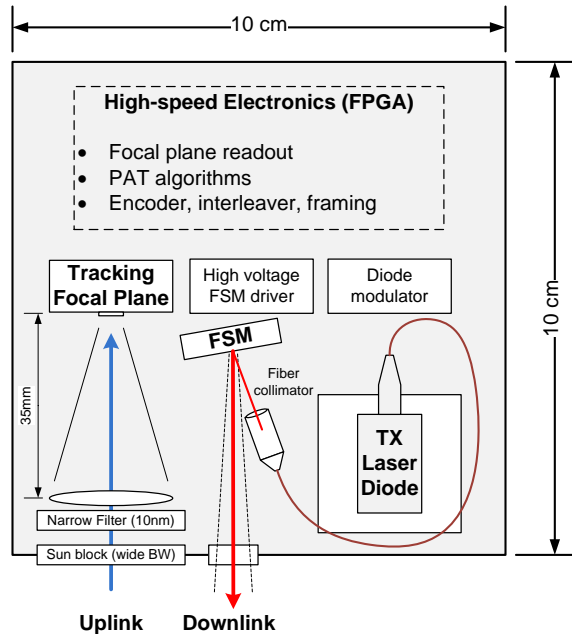


Figure 2: Notional optics layout, drawn roughly to scale.

We have chosen a “side-looking” configuration so that the FSO payload can be positioned anywhere within the CubeSat. In general, the ends of the CubeSat tend to be of high value for scientific payloads and ADCS sensors, so our side-looking configuration allows the FSO module to be placed in the middle. A second benefit of the side-looking configuration is that the spacecraft can perform its high-rate slew maneuver, which is needed during the FSO ground station pass, along the long axis of the satellite which typically has a smaller moment of inertia than the other two axes.

The uplink optical path is comprised of two filters, a lens system and a focal plane array which serves as the acquisition and tracking detector. The input aperture diameter is 25.4 mm, which was selected as a balance between collecting area and common size optical components. The lens system consists of a single element that has been selected to give the focal plane array a field of view of approximately 5 degrees, full cone angle. The focal length of the system is 35 mm.

Two optical filters are used on the uplink path to reject stray light which degrades tracking SNR and can produce unwanted thermal transients on the optical components. The outermost filter has a relatively wide bandwidth (100 nm) and rejects the majority of the harsh sunlight that can cause unwanted thermal transients inside the optical bench. The inner filter has a narrower bandwidth

(10 nm) and is critical for improving the focal plane’s imaging performance.

The downlink optical design is a simple “gimballed flat” configuration consisting of fiber-fed beam collimator followed by a 3.6 mm diameter MEMS fast-steering mirror (FSM). This system is designed to have a  $\pm 2.5$  degrees field of regard within which it delivers a 2.1 mrad (0.12 deg) divergent beam.

The gimballed flat design does not have any optical elements that follow the FSM. Most conventional FSO implementations would follow the fine-steering stage with beam expansion and collimation optics in order to meet microradian-scale divergence requirements. For our system, the target beam divergence is much larger: 2.1 mrad. A diffraction-limited aperture could be as small as 0.6 mm at our downlink wavelength of 975 nm while still meeting this divergence requirement. We use a commercial fiber beam collimator to produce a 1.0 mm diameter beam waist that has the desired 2.1 mrad divergence. The oversized 3.6 mm fast steering mirror diameter ensures that there is no beam spillover across the steering range.

### Pointing, Acquisition, and Tracking Subsystem

Given the limitations on the pointing accuracy of a CubeSat bus, a two-stage control approach is necessary to meet the FSO module pointing requirements. The FSO module does not place any requirements on what actuators or sensors the host ADCS uses, as long as the coarse stage meets the  $\pm 2.5$  degrees coarse pointing requirement. The available fine-stage options are to redirect the beam using a fast steering mirror (FSM), or to directly actuate the transmit fiber using a nutator. Based on available COTS components, a suitable FSM was chosen from a limited set of options (described below).

The uplink beacon is received at a 25.4 mm (1 inch) aperture, but the selected FSM has a diameter of only 3.6 mm. While a common transmit/receive path is highly desirable for control, the size of the FSM makes this extremely difficult. The beam must be resized prior to the FSM, but the resizing process causes beamwalk that exceeds the FSM diameter. The potential for beamwalk during resizing drives the bistatic optical layout described previously.

During the acquisition process, the ground station illuminates the satellite with a broad uplink beacon as closed-loop coarse control maintains the satellite bus within  $\pm 2.5$  degrees accuracy. From the spacecraft, the FSM also steers the downlink beam through the cone of uncertainty, and upon beacon detection the terminals close

the loop. The uplink beacon continues to be received by the FSO module's detector, and the signal is centroided to provide fine attitude knowledge. Once the link is acquired, the coarse control loop can be closed around the beacon detector, which provides much greater sensing accuracy to improve bus pointing.

Fine-stage control then provides additional correction to within  $\pm 210 \mu\text{rad}$ . Due to the bistatic design, there is no feedback mechanism to drive the FSM. Therefore, the FSM is driven open-loop based on the detector readout. Characterization of FSM performance, particularly during and after environmental/vibe testing is currently being reviewed.

## UPLINK DESIGN

The uplink optical signal exists purely for acquisition and tracking purposes. It does not carry communication data. Wavelength selection, particularly with respect to eye safety, was one of the primary design drivers for this portion of the FSO system. The sensitivity of the uplink beacon detector was a secondary factor.

The uplink system is designed to operate at a maximum range of 1000 km. This corresponds to approximately 20 degrees above the local horizon at our nominal 400 km LEO orbit. This value was selected as a compromise between low elevation angles, where atmospheric effects are severe, and high elevations angles where significant fractions of the pass would be "lost" prior to acquisition.

### *Key Parameter Selection*

For the uplink transmitter, the beam divergence angle is the most critical design parameter. It must be broad enough so that it reaches the satellite with high probability but not so broad that the transmit power requirements become unreasonable.

Since the beacon signal initiates the acquisition process, it must be pointed toward the spacecraft in an open-loop fashion using a priori information such as TLEs. Satellite position uncertainty and ground station pointing accuracy are the primary sources of uncertainty. However, our system is designed under the assumption that the host spacecraft does not include precision orbit determination capabilities (such as GPS). Instead, we have dimensioned the acquisition scheme so that it will work using NORAD-supplied ephemeris information.

In [4] a comparison is drawn between GPS-derived orbit propagation and conventional NORAD TLE prop-

agation. The results show that total position uncertainty of 2.164 km ( $3\text{-}\sigma$ ) for a CubeSat-size object in a 350 km LEO orbit can be obtained through TLE propagation. At a range of 1000 km this implies a pointing uncertainty of 2 mrad ( $3\text{-}\sigma$ ). The pointing uncertainty due to the ground station mount is still under investigation, but it is expected to be much less than the position uncertainty. To provide margin we have selected an uplink beacon divergence of 4 mrad.

On board the spacecraft, the beacon receiver has two design parameters that are of importance: field of view and spatial resolution. The field of view (FOV) of the beacon receiver must be sized in accordance with the coarse pointing performance of the host spacecraft. We assume the FOV to be  $\pm 2.5$  degrees which yields a high probability of detection when the spacecraft is attempting to acquire the beacon signal. The spatial resolution of the uplink beacon receiver determines how well the system can estimate the boresight offset (i.e. pointing error) of the incoming beacon signal. This spatial resolution needs to be at least as good as the downlink pointing accuracy of  $\pm 210 \mu\text{rad}$ .

### *Component Selection*

High-power lasers ( $> 500 \text{ mW}$ ) such as those needed for the uplink beacon are subject to eye safety restrictions as detailed in the ANSI Z-136 standard. This standard sets maximum permitted exposure limits that must be considered in the ground station design. Additionally, the open-air use of some lasers is governed by various FAA and NASA directives as they can constitute a distraction hazard to pilots. Systems which can cause a distraction hazard must incorporate appropriate safeguards (e.g. keep-out radar) which can drive up system cost and complexity. Operating in the non-visible wavelengths ( $> 800 \text{ nm}$ ) is advantageous as the signal is no longer considered a distraction hazard. Maximum permitted exposure (MPE) restrictions still must be observed but these can be met even with high power lasers through judicious selection of beam diameter.

Originally, we intended to use a 1550 nm uplink beacon. At this wavelength, high power laser amplifiers are readily available, MPE limits are relatively high and atmospheric effects are relatively benign. Unfortunately, detecting the 1550 nm signal on the spacecraft presents significant engineering challenges. Even though InGaAs devices (e.g. photodiodes and quadcells) have good responsivity at 1550 nm, these devices struggle to simultaneously provide wide FOV and high spatial resolution.

Often, these devices are used with a steering mechanism that allows a small FOV to be scanned across a much wider field of regard.

Focal plane arrays (FPAs) are capable of delivering both wide FOV and high resolution but aside from some exotic and power-hungry technologies, are not sensitive to 1550 nm photons. Most commercial FPAs are fabricated in silicon which has a long wavelength cutoff at about 900 nm. The availability of these devices has led us to an 850 nm uplink which is outside of human visual range (it isn't a distraction hazard) yet within the responsivity range of silicon and common FPAs.

Selection of a suitable FPA for this application is non-trivial. Obvious specifications of interest include: resolution, quantum efficiency (responsivity), pixel size, dark noise, read noise and power consumption. Lesser known parameters, which are still relevant to our design include: readout modes (e.g. "windowing"), complexity of readout circuitry, operational temperature range. Many manufacturers consider these aspects of their product's performance proprietary, and require NDAs before full datasheets can be obtained. It is also very common for these datasheets to provide extremely optimistic device parameters (e.g. read noise) that are only applicable under very specific operating configurations.

We reviewed FPAs from three manufacturers (Table 1). All of these devices are available in a monochrome version which lacks the Bayer filters that degrade performance in this application. For each array, the optical focal length needed to achieve a  $\pm 2.5$  degrees FOV was calculated.

A centroid-finding algorithm, similar to what is used in star trackers, is used to estimate the position of the beacon signal as projected onto the FPA. These algorithms are capable of sub-pixel resolution through use of a slightly de-focused spot. Performance of these algorithms is typically 0.2 pixels or better [8]. Given the above assumption, the focal length of the system, and the pixel size, it is possible to calculate the expected performance of the boresight estimate. These values, along with other detector parameters of interest are given in Table 1. All four of the FPAs evaluated are able to exceed the 210  $\mu\text{rad}$  boresight offset estimation requirement.

A secondary selection criteria for the FPA stems from the complexity of the circuitry needed to readout and process the pixel data from the device. Provided the offset estimation requirement can be met, there is little incentive to use a high resolution FPA. Lower resolution FPAs, such as the fourth unit evaluated ("FPA #4" in Table 1),

will generally be capable of high readout rates and tend to have higher QE than higher resolution FPAs.

Final selection of a FPA for this system is ongoing work, particularly with respect to the noise performance of the available detectors over their operating temperature ranges. We are in the process of obtaining detailed device information from the manufacturers on these parameters. We expect readout circuitry requirements to form the final selection criteria for the FPA.

### Performance Analysis

Even though the uplink channel does not carry data, the analysis approach that we have applied is very similar to that of a conventional communication link budget. This budget is used to predict the photon flux of both the beacon signal and the upwelling radiance of the Earth at the FPA. The FPA parameters, including dark current, read noise terms and an exposure time are used to predict the resulting image and SNR. We are currently assuming an upwelling radiance of ( $180 \text{ W m}^{-2} \text{ sr}^{-1} \mu\text{m}^{-1}$ ) which is consistent with sunlit clouds. This is a very conservative number given that the system will not be capable of operating through heavy cloud cover. Despite this strong background signal, the predicted beacon image still shows good contrast with the background (Figure 3). All four FPAs are capable of delivering  $> 20$  dB image SNR across a  $10 \text{ pixel} \times 10 \text{ pixel}$  region of interest.

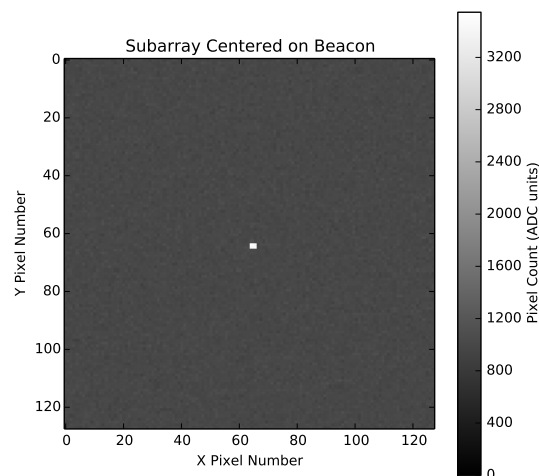


**Figure 3:** Simulated focal plane array image showing beacon signal (center) and noise contributions from upwelling radiance and detector noise (background).

**Table 1:** Comparison of focal plane array options. Vendor names and part numbers have been withheld intentionally.

	FPA #1	FPA #2	FPA #3	FPA #4
Resolution (pixels)	2048 x 2048	1920 x 1080	2592 x 1944	752 x 480
Size (mm x mm)	11.2 x 11.2	12.5 x 7.0	5.7 x 4.3	4.5 x 2.9
Pixel size ( $\mu\text{m}$ )	5.5	6.5	2.2	6.0
Quantum efficiency at 850 nm	30%	22%	15%	30%
Readout Windowing	Y-axis only	Unknown	Single XY window	Unknown
Focal length for 5x5 deg FOV (mm)	129	80	49	33
Centroiding performance ( $\mu\text{rad}$ )	8.5	16.2	9.0	36.4

## DOWNLINK DESIGN

The downlink subsystem consists of a compact high-power laser, collimation optics, and a fast-steering mirror (FSM). Given the stringent SWaP constraints faced in a CubeSat, the selection and specification of the laser and FSM have been given highest priority. In the sections that follow, we identify key parameters and discuss the selection of each of these components.

### *Key Downlink Parameters*

The downlink beam divergence angle is the most important parameter of the entire FSO payload. This value drives the attitude control requirements and determines the overall throughput of the communications link. Narrow transmit beams are what give FSO systems an edge over their RF counterparts so minimizing beamwidth is a top priority. If all other system parameters are held constant, a 10X reduction in beamwidth yields a 100X improvement in channel rate.

Wavelength is another important parameter in the downlink design. Water vapor and other atmospheric constituents cause severe attenuation at certain wavelengths so it is highly desirable to operate in a “window” where optical transmission is high [3]. The availability of high-power lasers and optical amplifiers also plays into wavelength selection.

### *Downlink Laser Selection*

The radiometric analysis presented earlier assumed that the FSO system must produce 1 W of optical power in order to achieve the desired link rate. This optical signal needs to have relatively narrow spectral width ( $< 10$  nm) so that an aggressive filter can be used at the receiving station to reject background light. Because of this spectral width requirement, light-emitting diodes (LEDs) are

not feasible. Instead, we must rely either on direct modulation of a high-power laser or a master-oscillator power amplifier (MOPA) architecture consisting of a source laser and an optical amplifier. Simultaneously, we must be mindful of the atmospheric transmission restrictions which confine operation to specific windows of the optical spectrum. Given laser availability and the atmospheric restrictions, we are mostly confined to the following non-visible wavelengths: 975 nm, 1064 nm and 1550 nm

At 975 nm a wide variety of “pump” lasers that are used as a component in fiber amplifiers are available commercially. These diodes have optical power outputs well in excess of our requirements and many boast “wall plug” efficiency exceeding 30%. Directly modulating these types of lasers at  $\sim 10$  MHz is a significant challenge but could likely be overcome with careful electrical design. One disadvantage of the direct modulation approach is that extinction ratios (ratio of light output between the “on” and “off” states) can be somewhat limited, degrading link performance.

At 1064 nm and 1550 nm MOPA architectures are the most common solution for high-power optical transmitters. In a MOPA design, a low-power source laser is modulated with the communications waveform. This signal is subsequently amplified by a fiber amplifier (Erbium or Yttrium-doped fiber amplifiers) to achieve the desired output power level. MOPA designs can produce superb extinction ratios and their modulation circuitry is simpler because modulation occurs at low power levels. The main disadvantage of MOPA designs is in their complexity, specifically the fiber amplifier which requires specialty fibers and a pump laser. Compact commercial fiber amplifiers are available but their “wall plug” efficiency is rarely higher than 15%.

The final selection of transmitter for the FSO design is still ongoing and we are pursuing both of the aforementioned transmitter technologies in parallel. An effort is



Sensor noise is included in the detector, which is modeled as white noise with an RMS error of 20% of the detector pixel size [8]. This approximation is conservative to ensure robustness. Additional error contributions include sensor noise from the gyroscopes as well as quantization, saturation, and delay of the input to the reaction wheels. Estimates of these parameters are modeled from the Maryland Aerospace MAI-400 [9]. The analog input to the FSM is also delayed and saturated.

The detector and gyroscope measurements are run through a Kalman filter to estimate the state. A PID controller is utilized for body pointing, with gains given by

$$K_p = J\omega_n^2 \quad (2)$$

$$K_d = 2J\eta\omega_n \quad (3)$$

$$K_i = K_p/10 \quad (4)$$

where  $K_p$ ,  $K_d$ , and  $K_i$  are the proportional, derivative, and integral gains respectively,  $\eta$  is the closed-loop damping ratio, and  $\omega_n$  is the closed-loop bandwidth. The closed-loop bandwidth is set at a factor of 100 below the sampling frequency of the loop, and the damping ratio is chosen to be 0.707 for good system response. The control loop for body pointing is run at 4 Hz, while the detector is sampled at 100 Hz to apply a correction with the FSM.

We model a satellite overpass to generate reference angles and slew rates to align with the ground station. The simulation uses a directly overhead pass and starts at a 20 degree elevation angle (at the ground station). Overhead passes are the most interesting case for analysis as they correspond with the highest possible slew rate. The coarse and fine pointing accuracy simulated in the time domain are shown in Figure 5.

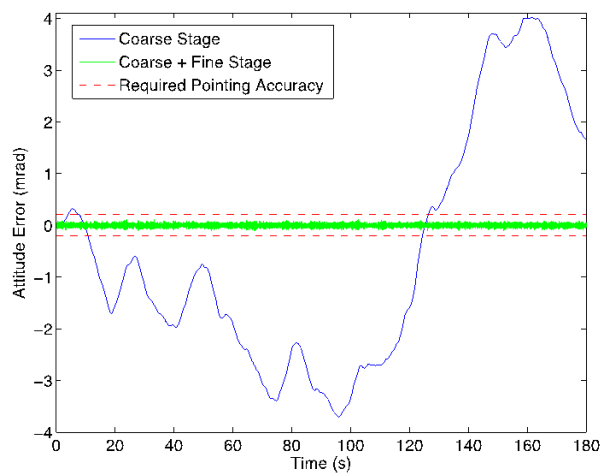


**Figure 5:** Downlink simulation results

The coarse stage, or body pointing, remains within a range of  $\pm 4$  mrad (0.23 degrees), with a RMS error of 2.3 mrad (0.13 degrees). Including the fine stage to correct errors in body pointing, the RMS error drops to  $\pm 25$   $\mu$ rad. Coarse pointing performance is expected to degrade when reaction wheel cross-coupling is accounted for, but the fine stage is still well within the required accuracy.

## CONCLUSIONS & FUTURE WORK

In this paper we have introduced the design of an FSO payload capable of fitting within the SWaP constraints of a CubeSat. The architecture of the system, including notable differences from conventional FSO systems have been described. The selection criteria for key optical and electronics components, such as the beacon detector and FSM, were presented along with simulation results confirming feasibility of critical portions of the system.

Despite this progress, there is still much room for improvement. The attitude control system simulation is being evolved into a 3-axis simulation that better captures the dynamics of the system. The downlink channel model is being refined to incorporate a specific detector technology, forward error correction and interleaving. The uplink/tracking channel will continue to be studied, particularly with respect to the impact of scintillation on the beacon signal. Finally, a “day in the life” simulation showing spacecraft and FSO link behavior through both acquisition and communication phases of operation is being developed.

In parallel with the simulation and analysis activities, we are also prototyping hardware in the lab to enable component characterization and link performance measurements. Final flight hardware decisions will be informed by both the higher fidelity simulations and lessons learned during lab prototyping activities.

## ACKNOWLEDGMENTS

The authors would like to acknowledge the Jet Propulsion Laboratory Strategic University Research Partnership Program (SURP) as well as the NASA Space Technology Research Fellowship program for funding this project. Additionally, we would like to thank Aaron Swank (NASA GRC) and William Farr (NASA JPL) for their valuable contributions and mentorship.

## REFERENCES

- [1] Michael Aherne, Tim Barrett, Lucy Hoag, Eric Teegarden, and Rohan Ramadas. Aeneas—colony i meets three-axis pointing. In *25th Annual AIAA/USU Conference on Small Satellites*, 2011.
- [2] B.E. Bingham and Q. Young. Road to a three-axis-stabilized cubesat. In *32nd Annual AAS Rocky Mountain Guidance and Control Conference*, volume 133, pages 607–613, 2009.
- [3] Abhijit Biswas and Sabino Piazzolla. The atmospheric channel. *Chap*, 3:121–213, 2006.
- [4] Brian G Coffee, Kerri Cahoy, and Rebecca L Bishop. Propagation of cubesats in leo using norad two line element sets: Accuracy and update frequency. In *AIAA Guidance, Navigation, and Control Conference*, 2013.
- [5] Siegfried Janson and Richard Welle. The NASA optical communication and sensor demonstration program. In *AIAA Small Satellite Conference*, 2013.
- [6] Brian Klofas and Kyle Leveque. A survey of cubesat communications systems: 2009-2012. In *CalPoly CubeSat Developers' Workshop*, 2013.
- [7] Edward Kneller, Kevin Hyer, Todd McIntyre, David Jones, and Charles Swenson. Cadet: A high data rate software defined radio for smallsat applications. In *26th Annual AIAA/USU Conference on Small Satellites*, 2012.
- [8] Carl Christian Liebe. Accuracy performance of star trackers—a tutorial. *Aerospace and Electronic Systems, IEEE Transactions on*, 38(2):587–599, 2002.
- [9] Maryland Aerospace Inc. *MAI-400 Reference Manual*.
- [10] Bogdan V Oaida, Matthew J Abrahamson, Robert J Witoff, Jessica N Bowles Martinez, and Daniel A Zayas. Opals: An optical communications technology demonstration from the international space station. In *Aerospace Conference, 2013 IEEE*, pages 1–20. IEEE, 2013.
- [11] C. Pong. *High-Precision Pointing and Attitude Estimation and Control Algorithms for Hardware-Constrained Spacecraft*. PhD thesis, Massachusetts Institute of Technology, 2014.
- [12] Christopher Pong, Matthew W Knutson, David W Miller, Sara Seager, Sungyung Lim, Timothy C Henderson, and Shawn D Murphy. High-precision pointing and attitude determination and control on exoplanetsat. In *AIAA Guidance, Navigation, and Control Conference*, 2012.
- [13] Bryan S Robinson, Don M Boroson, Dennis A Buri-aneek, and Daniel V Murphy. The lunar laser communications demonstration. In *Space Optical Systems and Applications (ICSOS), 2011 International Conference on*, pages 54–57. IEEE, 2011.
- [14] Karan Sarda, Cordell Grant, Stuart Eagleson, Daniel D Kekez, and Robert E Zee. Canadian advanced nanospace experiment 2 orbit operations: two years of pushing the nanosatellite performance envelope. In *ESA Small Satellites, Services and Systems Symposium*, 2010.

## APPENDIX A: SIMPLIFIED DOWNLINK RADIOMETRY

The radiometric link budget shown below was used in order to obtain an initial estimate for the minimum acceptable downlink beamwidth.

	Symbol	Value	Units	Notes
<b>Laser Transmitter</b>				
Laser electrical input power	PLD,elec	5	W	Electrical input power
Laser wavelength	$\lambda_{\text{peak}}$	1550	nm	Peak wavelength
Electro-optical efficiency	$\eta$	0.2	-	
Modulation duty cycle		0.5		Simple RZ for now
Laser avg. optical power	PLD,opt,avg	5.00E-01	W	
Laser avg. optical power (dBW)	PLD,opt,avg,c	-3.0	dBW	
Half-power beam width	$\theta_{1/2}$	0.120	degrees	Full cone angle where power is half of peak intensity
		2.100	mrad	
Solid angle of beam	$\Omega$	3.46E-06	sr	Assuming conical beam
Transmit antenna gain	Gt	3628217.069	-	Relative to $4\pi$ sr isotropic source
Transmit antenna gain (dB)	Gt,dB	65.60	dBi	
TX Radiant Intensity	Ie	7.22E+04	W*sr <sup>-1</sup>	Assumes half-power uniformly distributed across beam.
<b>Channel</b>				
Path length	d	1000	km	LEO at 400km can be tracked down to 20 degrees above horizon
Path loss (dB)	Lpath,dB	-258.2	dB	Standard free-space path loss equation
Atmpheric loss placeholder	Latm,dB	-6.00	dB	Placeholder value for absorbtion, scattering, turbulence
Power at receiver		-201.6	dBW	
Irradiance at receiver	Ee	1.81E-08	W*m <sup>-2</sup>	Calculated value, not used below
<b>Receiver</b>				
Aperture diameter		30	cm	
Receive antenna gain (dB)	Gr,dB	115.7	dB	Ideal (diffraction limited) gain
Power at detector	Prec,dB	-85.9	dBW	
Power at detector	Prec	1.28E-09	W or J/s	
Energy of single photon	Ephoton	0.00E+00	J	Uses transmitter wavelength from above
Photons per second		1.00E+10	photons/sec	
Required photons/bit		1000	photons/bit	An "easy" to build optical receiver
<b>Predicted data rate</b>		<b>10.00</b>	<b>Mbps</b>	